ORIGINAL PAPER

Homology model of nonmuscle myosin heavy chain IIA and binding mode analysis with its inhibitor blebbistatin

Yanni Lv · Shuai Lu · Tao Lu · Junping Kou · Boyang Yu

Abstract Nonmuscle myosin heavy chain IIA (NMMHC IIA, gene code: MYH9) plays a critical role in physiological and pathological functions. A homology model of NMMHC IIA was constructed based on the crystal structure of smooth muscle myosin II. Blebbistatin, a myosin II ATPase inhibitor, had been found to bind to NMMHC IIA with Leu228 as the important amino acid residue and van der Waals contacts as the main force of the interaction. The final complex demonstrated that the destruction of the salt bridge occurred between the Arg204 and Glu427 residues when blebbistatin was present. Molecular dynamic simulation of the complex showed that the binding affinity of blebbistatin to NMMHC IIA was strongly sensitive to the nucleotide binding region and actin binding region. The disturbance of the two regions increased the enhancement of the binding cavity with blebbistatin and resulted in a slightly more expanded conformation in the nucleotide binding region and actin binding region. A combined pharmacophore- and docking-based virtual screening was performed to identify several saponins as potential inhibitors for NMMHC IIA. These findings introduce new insights on the binding mode of blebbistatin and NMMHC IIA and novel leading compounds from natural products for NMMHC IIA-related diseases.

Y. Lv · J. Kou (✉) · B. Yu (✉)
State Key Laboratory of Natural Medicines, Department of Complex Prescription of TCM, China Pharmaceutical University, 639 Longmian Road,
Nanjing 211198, People's Republic of China
e-mail: junpingkou@163.com
e-mail: boyangyu59@163.com

S. Lu · T. Lu
Department of Organic Chemistry, China Pharmaceutical University, Nanjing 211198, People's Republic of China

Introduction

Myosin is the main motor protein in many muscle organs, and its interaction with actin is a key process in many physiological and pathological functions. Most myosins belong to class II, whose major function is to supply contractile force for muscles. Myosin II can be divided into muscle protein II and nonmuscle protein II [1]. There are three subtypes of nonmuscle myosin II: nonmuscle myosin IIA, B and C, coded by three different genes named MYH9, MYH10 and MYH14 in humans [2]. Nonmuscle myosin IIA (NMMHC IIA) is the primary subtype and plays a fundamental role in cell adhesion, migration, proliferation and differentiation [3, 4], etc. NMMHC IIA has recently been proposed to be a potential target for various diseases. The role of myosin in platelet contractile phenomena and outside-in signaling accounts for the strong hemostatic defects observed in mice with disruption of MYH9 [5]. It might also act as an HSV-1 entry receptor and a new target for antiviral drug development [6]. A recent study demonstrated that over-expression of let-7f in gastric cancer could inhibit invasion and migration of gastric cancer cells through directly targeting the tumor metastasis-associated gene MYH9 [7]. Moreover, the activation of myosin II could also promote autophagosome formation during starvation [8]. Our previous study also identified NMMHC IIA as a potential target of cardio cerebral vascular diseases based on a molecular probe from a natural product [9]. Thus, NMMHC IIA is responsible

for transmitting and regulating targets in signaling pathways.

It is widely accepted that inhibitors can be a useful tool in illuminating the function of proteins. As an inhibitor of myosin II ATPase activity [10, 11], blebbistatin is commonly used to explore the function of NMMHC IIA [12–15]. Blebbistatin was recently found to inhibit the interaction of actin-myosin in isolated contractile proteins [16]. The X-ray crystal structure of Dictyostelium discoideum myosin II gave a clear description of the active cavity and the interaction mode of blebbistatin with myosin II [17]. The blind docking of blebbistatin on the myosin head elucidated the structural basis of the interaction of switch I with blebbistatin [11]. However, there have been few detailed reports about the interaction mechanism between blebbistatin and NMMHC IIA. Moreover, other novel or specific NMMHC IIA inhibitors are of great interest to explore due to NMMHC IIA's important role in many diseases.

Virtual screening is rapidly becoming a popular alternative to high throughput screening because it is less time consuming and allows researchers to narrow the search to a relatively small set of promising compounds [18]. Structure-based virtual screening methods might improve the probability of identifying hits using a process that generates queries from ligand-receptor interaction information followed by cluster analysis coupled with the exclusion volumes. Meanwhile, a combined pharmacophore- and docking-based virtual screening attempted to better identify the potential inhibitors for NMMHC IIA. Protein homology modeling is currently the most accurate method for the prediction of three-dimensional structure models. In the present study, we constructed a homology model of NMMHC IIA and used molecular dynamic simulation to analyze the interaction mechanism of blebbistatin and NMMHC IIA. We found that the formation of the salt bridge and the change of functional regions were index of functional alteration, and we carried out a combined pharmacophore- and docking-based virtual screening against NMMHC IIA, which resulted in a series of compounds with predictive noticeable inhibition from natural products. These findings shed new light on the binding mode of blebbistatin and NMMHC IIA and on novel leading compounds for NMMHC IIA-related diseases.

Materials and methods

Homology modeling and refinement of protein

The blast searches by Discovery Studio2.5 (Accelrys Inc., San Diego, CA) [SP1] and Sybyl6.9 (Tripos Inc., St.
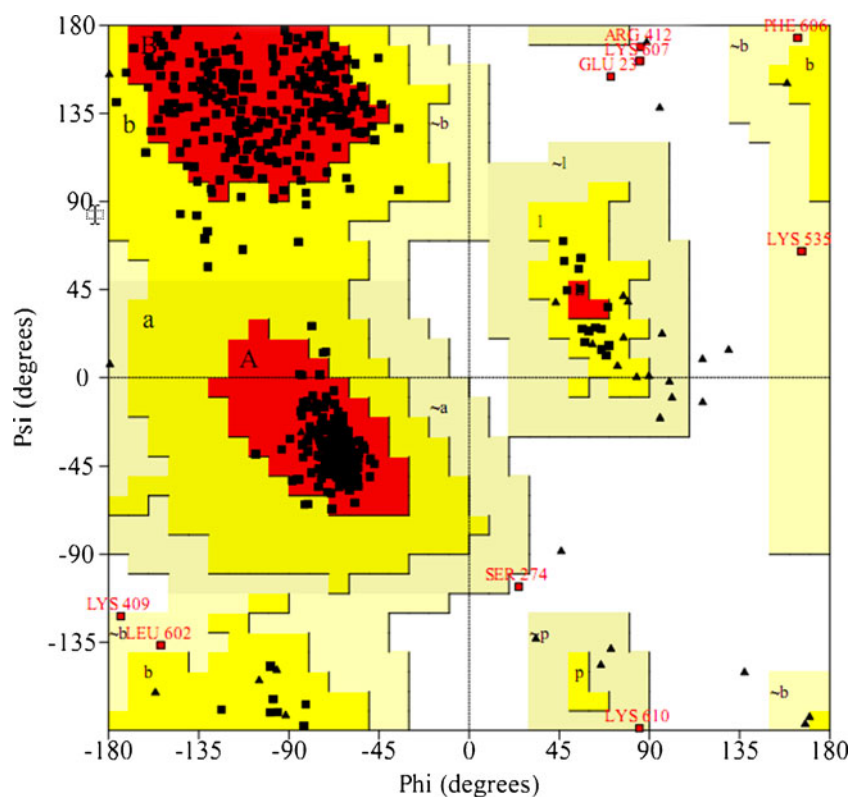
Louis, MO) [SP2] both showed that PDB: 1BR2 was the most homologous protein to NMMHC IIA. PDB: 1BR2 represented the visualization of the pre-power stroke state with the resolution of 2.9 Å. Sequence alignment showed that the whole sequence of NMMHC IIA exhibited quite high 74.0 % identity and 81.8 % similarity to 1BR2 (Fig. 1). NMMHC IIA sequence was downloaded from the UniProt protein knowledge database with accession number P35579; the finder template was downloaded from the RCSB protein data bank. The functional region shared a series of highly conserved key residues in the nucleotide binding region (139–146) and actin binding region (551–573) (Fig. 1). A three-dimensional structural model was constructed based on the corresponding domains of 1BR2. Multiple alignments were implemented between 1BR2 and NMMHC IIA by clustal x1.83 of Vega zz2.2.0 [SP3]. The three-dimensional structure model of NMMHC IIA was generated by Discovery Studio2.5. The insertions of the target sequence were dealt with as loops. Twenty basic models, qualified by probability density function energy (PDF energy), were generated at last. And the discrete optimized protein energy (DOPE energy) score based on statistical potentials was employed as another strategy to measure the quality, when the PDF energy values were extraordinarily close to each other. Finally, the model with the lowest PDF energy (3,097.87) and DOPE score (−55,459.3) was adopted for next study. For the purpose of refinement, all simulations were carried out using MD software package Gromacs3.3 on an IBM System X3400 [SP4] server with the Amber03 force field. Subsequent MD simulations were first performed under a 50 ps tethered MD simulation followed by a 4 ns untethered MD simulation until balanced. The temperature was kept constant at 300 K under coupling isotropic pressure. The structure was solvated with water molecules in a cubic simulation box (9×9×9 nm). Chloride ions were added as counter ions to provide eletroneutrality. An integration time step of 2 fs was used. Electrostatic and van der Waals contacts were dealt with, respectively, by the particle mesh Ewald (PME) method and the truncated value method (cut-off) process. All bond lengths were constrained using the LINCS algorithm.

Pose validation, molecular preparation and docking

Considering different state and sequences of the myosin models, the binding cavity was found by assistant methods based on the literature data [17]. The precise binding cavity was determined via CH_3 probe by Q-sitefinder [SP5] and blind docking by Autodock3.05 [SP6]. Blebbistatin was extracted from 1YV3 and applied to all hydrogens and Gastiger-Huckel charges in Sybyl in the

Fig. 1 Alignments implemented between PDB: 1BR2 and NMMHC IIA by clustal x1.83 of Vega zz2.2.0. Red spheres represented alignments for nucleotide binding region and blue spheres represented alignments for actin binding region

```
NMMHC II A    MAQQAADKYLYVDKNFINNPLAQADWAAKKLVWVPSDKSGFEPASLKEEVGEEAIVELVE    60
1BR2          ----------------------------LVWVPSEKHGFEAASI------EVTVELQE    24
                                          ******:* ***.**:     *. *** *

NMMHC II A    NGKKVKVNKDDIQKMNNPPKFSKVEDMAELTCLNEASVLHNLKERYYSGLIYTYSGLFCVV    120
1BR2          NGKKVTLSKDDIQKMNNPPKFSKVEDMAELTCLNEASVLHNLRERYFSGLIYTYSGLFCVV    84
              *****.:.*********************************:***:*************

NMMHC II A    INPYKNLPIYSEEIVEMYKGKKRHEMPPHIYAITDTAYRSMMQDREDQSILCTGESGAGK    180
1BR2          INPYKQLPIYSEKIIDMYKGKKRHEMPPHIYAIADTAYRSMLQDREDQSILCTGESGAGK    144
              *****:******:*::.*************************:***************

NMMHC II A    TENTKKVIQYLAYVASSHKSKKDQGELERQLLQANPILEAFGNAKTVKNDNSSRFGKFIR    240
1BR2          TENTKKVIQYLAVVAS--------GELEKQLLQANPILEAFGNAKTVKNDNSSRFGKFIR    196
              ************ ***        ****:***********************

NMMHC II A    INFDVNGYIVGANIETYLLEKSRAIRQAKEERTFHIFYYLLSGAGEHLKTDLLLEPYNKY    300
1BR2          INFDVTGYIVGANIETYLLEKSRAIRQAKDERTFHIFYYLIAGASEQMRNDLLLEGFNNY    256
              *****.*********************:*********** :**.*:::.***** :*:*

NMMHC II A    RFLSNGHVTIPGQQDKDMFQETMEAMRIMGIPEEEQMGLLRVISGVLQLGNIVFKKERNT    360
1BR2          TFLSNGHVPIPAQQDDEMFQETLEAMTIMGFTEEEQTSILRVVSSVLQLGNIVFKKE---    313
              *******.**.***:.******:*** ***: **** .:***:*.************

NMMHC II A    DQASMPDNTAAQKVSHLLGINVTDFTRGILTPRIKVGRDYVQKAQTKEQADFAIEALAKA    420
1BR2          -QASMPDNTAAQKVCHLMGINVTDFTRSILTP----------KAQTKEQADFAIEALAKA    362
              *********.**:**:*********.****           ******************

NMMHC II A    TYERMFRWLVLRINKALDKTKRQGASFIGILDIAGFEIFDLNSFEQLCINYTNEKLQQLF    480
1BR2          KFERLFRWILTRVNKALDAS------FLGILDIAGFEIFEINSFEQLCINYTNEKLQQLF    416
              .:**:***:: *:***** :       *:***************:*************

NMMHC II A    NHTMFILEQEEYQREGIEWNFIDFGLDLQPCIDLIEKPAGPPGILALLDEECWFPKATDK    540
1BR2          NHTMFILEQEEYQREGIEWNFIDFGLDLQPCIELIERPTNPPGVLALLDEEC----ATDT    472
              *********************************:***:*. ***:*******    ***.

NMMHC II A    SFVEKVMQEQGTHPKFQKPKQLKDKADFCIIHYAGKVDYKADEWLMKNMDPLNDNIATLL    600
1BR2          SFVEKLIQEQGNHAKFQK-----SKTEFCILHYAGKVTYNASAWLTKNMDPLNDNVTSLL    527
              *****::****.*.****     .*::***:****** :*. ** *********::.**

NMMHC II A    HQSSDKFVSELWKDVDRIIGLDQVAGMSETALPGAFKTRKGMFRTVGQLYKEQLAKLMAT    660
1BR2          NQSSDKFVADLWK----------------------------RTVGQLYKEQLTKLMTT    557
              :*******::.***                            ***********:***:*

NMMHC II A    LRNTNPNFVRCIIPNHEKKAGKLDPHLVLDQLRCNGVLEGIRICRQGFPNRVVFQEFRQR    720
1BR2          LRNTNPNFVRCIIPNHEKRAGKLDAHLVLEQLRCNGVLEGIRICRQGFPNRIVFQEFRQR    617
              ******************:*****.****:******************:********

NMMHC II A    YEILTPNSIPKGFMDGKQACVLMIKALELDSNLYRIGQSKVFFRAGVLAHLEEERDLKIT    780
1BR2          YEILAANAIPKGFMDGKQACILMIKALELDPNLYRIGQSKIFFRTGVLAHLEEERD----    673
              ****:.*:************:*********.*********:***:***********
```

tripos force field under an implicit solvent environment. The minimization steps included 1000 cycles of steepest descent until satisfying the convergent threshold of 0.05 $kcal^{-1}\cdot\text{Å}^{-1}$. Initial complex conformation was generated based on Glide4.5 (Grid-based ligand docking energetics4.5) (Schrödinger LLC, New York, NY, USA) [SP7] program. The steps were as follows: Blebbistatin and homology model of NMMHC IIA were prepared using ligprep and protein preparation wizard in Maestro 8.0 [SP7] adding hydrogen atoms and desalting. The next step comprised the grid generation performed by box size (32×32×32 Å). In this step a distinct area of the structure was defined, in which the docking was performed. The grid box was manually positioned to comprise the whole ligand binding site. The docking step was performed using the generated grid files and the prepared ligands, with the advanced option set as 14×14×14 Å. The initial complex conformation was subjected to further molecular minimization by Gromacs3.3 on an IBM system X3400 server in the AMBER03 force field environment. Topology parameters were self-generated by the Dundee Prodrg2 server. The

same steps described for optimizing protein alone were also used for bound complexes. Molecular graphics were inspected in molecular virtual viewer1.2.0 (Molegro) [SP8] and Discovery Studio; two-dimensional figures were created in Excel and Grace.

Virtual screening for novel inhibitors

Current ligand-based computational methods often ignore the intricate details of binding site shapes and focus only on the key pharmacophore elements as the query. Thus, they often miss critical information during the virtual screening process, resulting in an increased number of false positives. Structure-based virtual screening methods, which seek to find effective means to utilize experimental receptor structure information, have been reported recently. These methods can be coupled with interaction data to improve the probability of identifying hits. They use a process that generates queries from ligand-receptor interaction information followed by cluster analysis to identify the best set of spheres to represent the shape of the binding site. Binding site exclusion volumes are also considered during the virtual

screening process. These methods are thus designed to increase the efficiency of database searching while taking into account the topographical constraints of the target binding site to help reduce the false positive rate. Meanwhile, docking studies attempted to include the possible interactions at the binding site, thus further screened the candidate molecules. Then the binding mode of blebbistatin to NMMHC IIA was defined by the interaction pattern of its pharmacophore. The results were clustered to two features to identify the best pharmacophoric features by the common feature pharmacophore generation module. The features involved two hydrogen bond acceptors, hydrogen bond donors and hydrophobic groups. The exclusion model was defined using C atoms with a radius of 10Å around the query. The final structure-based query was put into an in-house natural products drug database containing 12,006 molecules to screen potential inhibitors. In the docking study, the returned hits of the candidate molecules were prepared using the ligprep module in Maestro8.0. The structure of homology model of NMMHC IIA was prepared using the protein prepare wizard to generate the grid file. The grid generation was performed by box size (32×32×32 Å). The sets of compounds were evaluated using Glide in the precise mode. The precise docking provided an accurate score and rank for docked compounds. G-score was used to score and rank the docked compounds for Glide.

Results and discussion

Analysis of homology model and binding cavity of NMMHC IIA

The refined homology model of the minimized model was confirmed to have reasonable residue distributions with approximately 91.9 % favored residues according to the Ramachandran plot (Fig. 2), while disfavored residues were located away from the cleft region [SP9]. The Profile-3D score of the model (312.8) was over the expected low score (153.874) and was 83.00 % of the expected high score. This close alignment allows for the production of a rational homology model of NMMHC IIA. Docking results showed a good fit with the green lyophobic grids of the potential active cavity predicted by Q-sitefinder. Most of the top sixty molecules via Autodock were located near or at the interface of the cleft region (Fig. S1).

Trajectory analysis of blebbistatin with NMMHC IIA

As shown in Fig. 3, the global heavy atom RMSD of the complex was larger than that of the protein alone in the first 500 ps. This difference showed the structural change initiated by blebbistatin. After 500 ps, the RMSD clearly showed that the complex conformation became smaller during the dynamic process compared with the starting

Fig. 2 Ramachandran plot of NMMHC IIA generated by Procheck
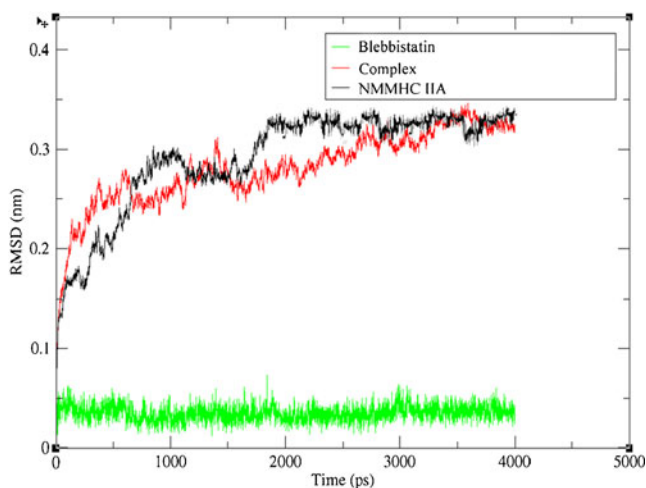
Fig. 3 RMSD for heavy atoms of blebbistatin (*green*), NMMHC IIA (*black*), and the complex (*red*) of blebbistatin and NMMHC IIA during the molecular dynamic simulation

structure. Blebbistatin limited the flexibility of surrounding residues during interactions with them. We performed these simulations to determine the possible interaction mechanism for conformational change. Although the protein appeared rigid as a whole, the binding of inhibitor was very sensitive to functional domains. The complex of blebbistatin and NMMHC IIA balanced after 2000 ps, as reflected by the small overall RMSD values. The final complex conformation extracted during 2000–3000 ps was used for further analysis and experimental verification.

To compare the relative disturbance of blebbistatin at the NMMHC IIA binding site and to assess its contribution to the conformational change of functional regions, we measured the deviations from the original complex structure of blebbistatin and NMMHC IIA (Fig. 4). As in the case of X regions, we measured the change of RMSD between atoms Glu201 and Ser203 (201–203) during the molecular dynamic simulation. The X region was observed to depart with RMSD 0.2149 Å. In the crystal structure of the active A, B and C regions (all positioned close to the nucleotide binding region), the RMSD of Phe400 and Phe405 (400–405) was 0.2587 Å, Asp171 and Ser174 (171–174) was 0.2345 Å, Ser117 and Gly120 (117–120) was 0.2924 Å. The D region of the actin binding region including Lys619 and Lys623 (619–623) was altered with RMSD 0.3212 Å. Knowing that the overall superimposition RMSD of Cα of NMMHC IIA is 0.1665 Å, these differences show that the structural changes started after binding with blebbistatin. This finding suggests that the binding affinity of blebbistatin with NMMHC IIA was strongly sensitive to active functional domains. Although the binding cavity was at a relatively far distance from the actin binding region, binding with inhibitors resulted in destabilization of local conformational regions. The disturbance of the functional regions increased the enhancement of the binding cavity with blebbistatin and acquired a slightly more expanded conformation in the nucleotide binding region and actin binding region. We intended to research the complex of the actin-NMMHC IIA-inhibitor further with a longer molecular dynamic study.

Fig. 4 Main differences between the Cα positions of the structure of complex (*gray*) and optimized complex (*pink green*) after refinement. The salt bridge figure represented the comparison of the H-bond distance between Arg204 and Glu427 before (*deep green*) and after (*pink green*) the molecular dynamic simulation. The sky blue misty spheres represented the nucleotide binding region, the green misty spheres represented the actin binding region and the purple spheres represented the conserved pre-stroke pathway [27]

Analysis of interaction residues and forces

Low RMSD was obtained by the superposition of NMMHC IIA with the crystal structure of 1YV3 (RMSD: 0.1844). The key conserved residue Leu228 formed the same H-bond with the hydroxyl group of blebbistatin, which was almost identical to Leu262 in 1YV3 (Fig. 5). Leu228 achieved the highest frequency of occurrence in H-bond, van der Waals contacts, hydrophobic forces among interacting residues as determined by the Molegro software (Fig. 5) (Table 1). Energy terms of Xscore [SP10] indicated that van der Waals and contacts were the main interaction forces. Except for constant items, van der Waals contacts took 61.2 %, 72.93 % and 57.63 % of the total scores in HPscore, HSscore and HMscore, respectively.

Virtual screening for novel inhibitors of NMMHC IIA

A total of 147 compounds were returned as the hits from 12,006 molecules from an in-house database. Then 147 molecules were evaluated using Glide to rank the molecules. Fifty two molecules owned the higher docking scores compared with G-score (−27.7446) between the reference molecule blebbistatin and NMMHC IIA. The top ten hits returned from structure-based virtual screening were shown in Table 2. The stem nuclei belonged to a large group of compounds arranged in a four or five ring configuration of carbons. The hits mostly belonged to the group of saponin compounds mainly triterpenoid saponin, such as ganoderic acid I, lucidenic acid B, digitoxin, proscillaridin A and protopanaxatriol. The two top docking ranked molecules (ganoderic acid I and protopanaxatriol) showed a good fit with all the features of the pharmacophore. Compound 1 (CAS no. 98665-20-4; ganoderic acid I): 3-hydroxyl was mapped by hydrogen bond donor pharmacophore well. The hexatomic ring consisting of atoms 8, 9, 11, 12, 13 and 14 was fitted by hydrophobics pharmacophore. 11-carbonyl was fitted by hydrogen bond acceptor pharmacophore, while the 27-carboxyl was fitted by hydrogen bond acceptor pharmacophore (Fig. 6a-1). Compound 2 (CAS no. 1453-93-6; protopanaxatriol): 3-hydroxyl was mapped by hydrogen bond donor pharmacophore well. The hexatomic ring consisting of atoms 8, 9, 11, 12, 13 and 14 was fitted by hydrophobics pharmacophore. 12-hydroxyl was mapped by hydrogen bond acceptor pharmacophore, while the ethylenic linkage between 24 and 25 atoms was mapped by the hydrophobics pharmacophore (Fig. 6b-1).

To understand the mechanism and to aid future lead optimization studies, we performed docking on the two most potential compounds with the homology model of NMMHC IIA in Maestro8.0. As shown in Fig. 6a-2, compound 1 bound to the cleft region via two hydrogen bonds

Fig. 5 Blebbistatin binding cavity and contact residues for NMMHC IIA. a Key residue interacting with blebbistatin. b The complex conformer via Glide docking. Different colors represented the region according to the KD. Blebbistatin is shown by CPK style in dark blue. c 5 Å residues around the blebbistatin binding site. (C-1): H-bonds were marked with dashed green lines; (C-2): van der Waals contacts were marked with dashed violet lines; (C-3): hydrophobic forces
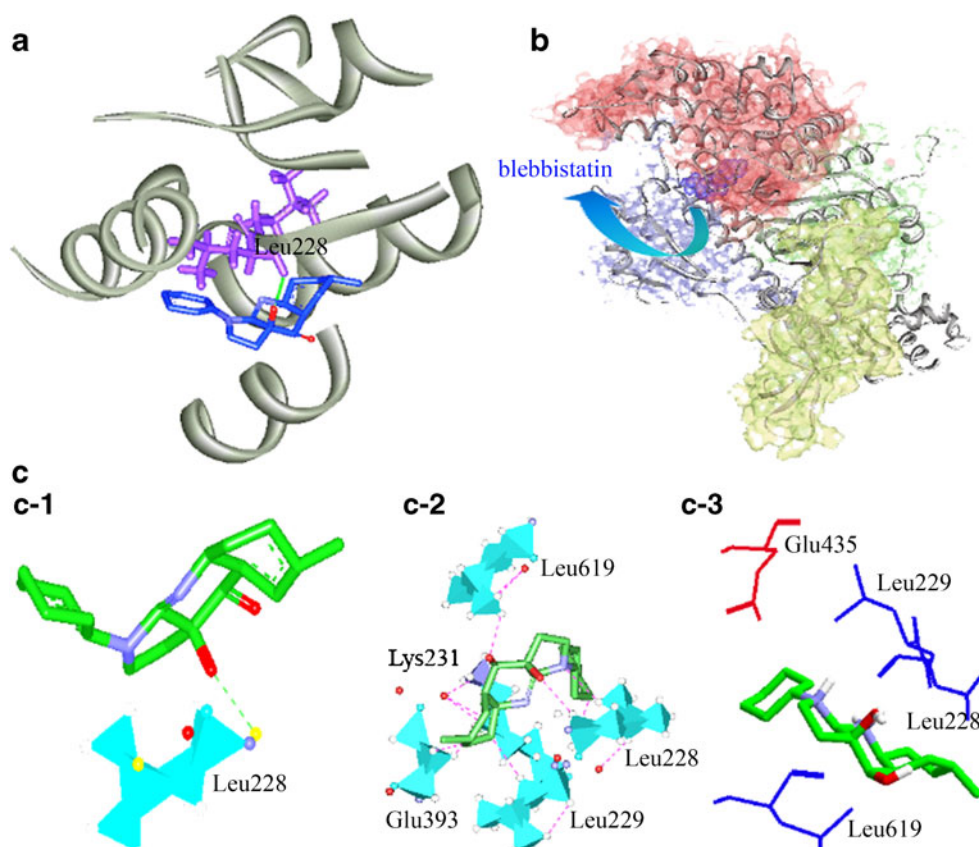
Table 1 The interacting residues analyzed by the Molegro molecular viewer

Residue	ID	Total energy (kJ mol^{-1})
Lys	231	−4.2817
Leu	228	−4.0409
Leu	229	−3.7546
Val	616	−2.7039
Glu	393	−1.6931
Tyr	620	−1.5330
Lys	557	−1.2093
Glu	435	−1.1224
Arg	397	−1.0791
Phe	434	−1.0212
Leu	619	−0.9916
Glu	230	−0.5621
Thr	226	−0.4373
Tyr	227	−0.3043
Gln	623	−0.1769
Ser	232	−0.1394
Asp	560	−0.1104
Cys	438	−0.1033
Phe	396	−0.1006
Gly	617	−0.0928

Table 2 Top ten hits returned from virtual screening
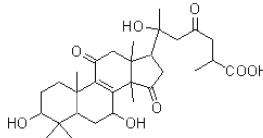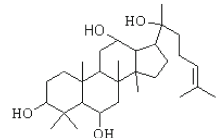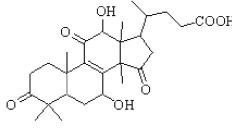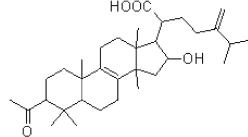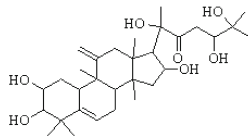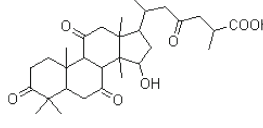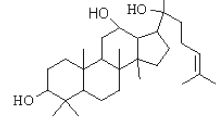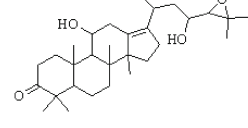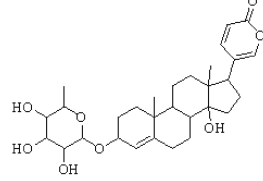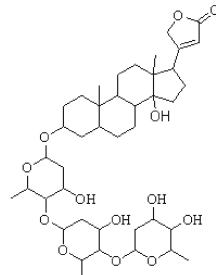
CAS number	Compound	Pharmacophore fit value	Docking G-score
98665-20-4		4.297	-31.1084
1453-93-6		4.187	-31.0943
95311-95-8		3.167	-31.0931
29070-92-6		3.354	-31.0712
156667-10-6		3.174	-31.0410
400604-10-6		3.398	-30.6828
6892-79-1		3.417	-30.5109
18649-93-3		3.023	-30.0141
466-06-8		3.568	-29.9610
71-63-6		3.498	-29.8675

from the 7-hydroxyl of Lys231 and the carboxyl of Gln623. Compound 2 (Fig. 6b-2) formed three hydrogen bonds from the 3-hydroxyl of Lys231, 12-carboxyl of Leu229 and 20-hydroxyl of Thr226. These interactions could as least partially stabilize the conformation of the substituted residues. Likely, the tetracyclic triterpene stem nuclei of both compounds arranged in a four ring configuration of carbons pointed into the cleft region, while it appeared to interact by the strong hydrophobic interactions with surrounding residues.

Discussion and conclusions

Its close relationship with various diseases implies that NMMHC IIA might be a potential target and transmitter in physiology and pathology. There is a dire need to explore the interaction mechanism between blebbistatin and NMMHC IIA. However, because there is no crystal structure of NMMHC IIA available, a homology model structure of NMMHC IIA was built with the crystal structure of 1BR2 due to the high identity and the suitable state for analysis. The obtained model was consistent with the results of residue distribution experiments. This observation suggests that the homology model is useful for experimental studies on the interaction mechanism between blebbistatin and NMMHC IIA. Blebbistatin was traced to the region distant

Fig. 6 Pharmacophore mapped by compound 1 (A-1) and 2 (B-1). Stick representations of compounds 1 and 2. Pharmacophore features were color coded as follows: cyan spheres: hydrophobics, green spheres: hydrogen bond donor, red spheres: hydrogen bond acceptor and gray spheres: exclusion volume. Binding models in homology model of NMMHC IIA from docking for compounds 1 (A-2) and 2 (B-2). Stick representations of compounds 1 and 2 in the homology model of NMMHC IIA cavity. The hydrogen bond was shown as a green dashed line
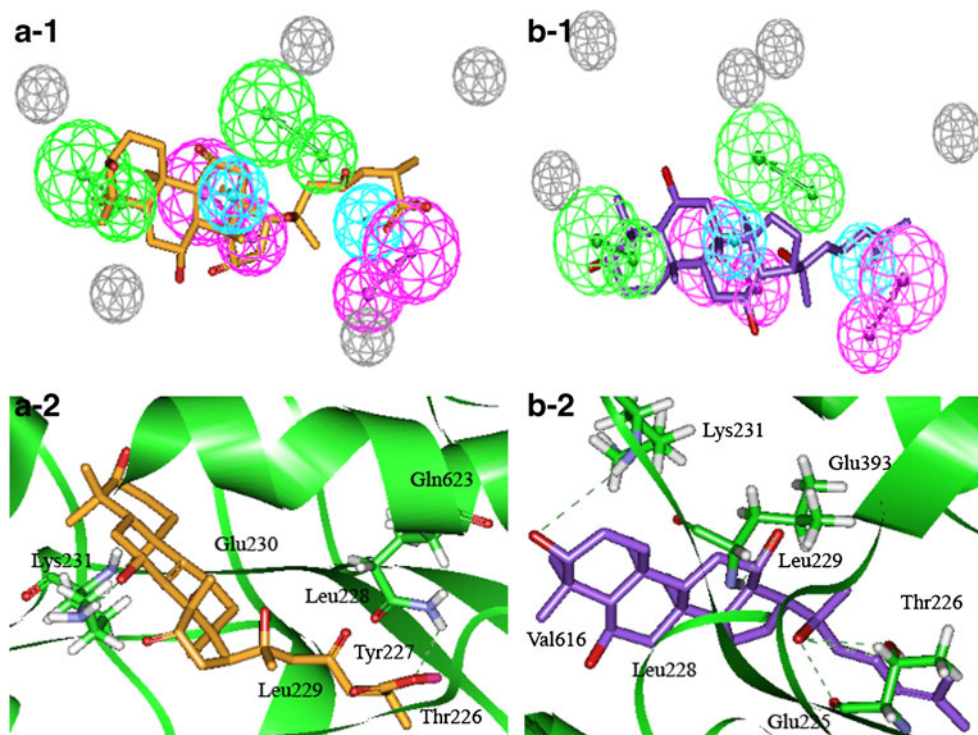
from the nucleotide binding region and actin binding region. However, blebbistatin resulted in a functional conformational change that is characteristic of noncompetitive inhibitors [10]. In noncompetitive inhibition, the inhibitor binds to an enzyme at a site other than the active site and reduces the activity of the enzyme whether it has already bound the substrate. Therefore, blebbistatin was considered not only noncompetitive with the substrate of ADP or ATP, but also of importance to the function of ATPase at relatively distant sites.

We needed to investigate how blebbistatin exerted effects on relatively distant functional regions. The process of myosin and its inhibition by blebbistatin was monitored by molecular dynamic simulation. The simulation time should be able to observe the changes responsible for the illumination of the mechanism. The formation of the salt bridge had the changes within 1.25 ns simulation [19, 20]. Computational results showed the role of water molecules in regulating the formation of the salt bridge within 1 ns [21]. The disturbance signal extended over the motor domain in 150 ps and induced slowly varying collective motions of atoms at the actin binding site and the junction with the neck [22]. Combined with those two parts, enough conformational changes would be expected in 4 ns to justify the conclusions. The myosin templates differentiate in their active and inactive forms that are important for the next docking analysis and molecular dynamic simulation. PDB: 1BR2 presents a description of the visualization of the pre-power stroke state as well as the highest identity. Meanwhile, blebbistatin showed a great affinity for the blocked state of

the motor head region [11] under the pre-stroke state, and blebbitatin may only form the salt bridge when the receptor is under the pre-stroke state. Thus the three-dimensional homology model might be constructed based on the corresponding domains of 1BR2 with the visualization of the pre-power stroke state [23]. The accurate state for the homology model would be meaningful for illuminating the action mechanism for the blebbistatin. We proposed that binding with blebbistatin could stabilize the conformation of the motor head region [17] and hinder the formation of the salt bridge. The blebbistatin with high binding affinity strongly stabilized the head conformation in the pre-stroke state [24]. Based on the two water molecules hypothesis [25], residues of Arg in switch-1 and Glu in switch-2 [26] tilted toward each other to quickly form a stable salt bridge from 6 Å to 3 Å during the recovery state transition to the stroke state [19]. The salt bridge facilitates ADP, Pi and energy [27], promoting the power-stroke state by providing a favorable cavity for ATP hydrolysis (Fig. 3). The existence of the inhibitor might hinder two key residues from approaching to form the salt bridge. Arg204 and Glu427 shifted slightly from the original position of 8.335 to 8.234 (Fig. 2), rather than the 3 Å of the salt bridge. The formation of the salt bridge differed from that under the active form that was destroyed by the combination with blebbistatin having an influence on ATP hydrolysis. The inhibition mechanism of bebblistatin for the ATPase in the NMMHC IIA could be explained that it hinders the formation of the salt bridge, thus unfavorable for ATP hydrolysis.

Although functional regions (inhibitor binding cavity, nucleotide binding region and actin binding region) are rather different in their position numbers, they are spatially in close proximity and can interact with each other [17]. The effect of the disturbance due to ATP hydrolysis in the nucleotide binding pocket was found to spread throughout the myosin head in the form of modulation of thermal fluctuations [28]. The signal was transmitted to the tail part of myosin and induced large swinging deviations of the converter and generated an external force when the lever arm was fixed to a heavy filament. Five regions (A, B, C, D and X) positioned, respectively, close to the inhibitor binding cavity, nucleotide binding region and actin binding region were observed to have conformational alterations with large deviations of RMSD. We deduced that the integrated signals acting on the converter or lever arm should include an extra conformational disturbance induced by binding with blebbistatin. In sum, blebbistatin was fundamental in hindering the formation of the salt bridge and inducing a conformational disturbance, resulting in the functional alteration of ATP hydrolysis and large deviations of the converter and lever arm.

Due to the features of noncompetitive inhibitors, the hits obtained from the virtual screening were likely to possess a wide variety of structural characteristics. The pharmacological functions of Chinese herbal remedies were more widespread than those of western drugs. It is therefore important to screen novel inhibitors from the database derived from natural sources. The results of the combined pharmacophore- and docking-based virtual screening showed that the hits mostly belonged to the group of saponin compounds. There were mainly two kinds of structures including tetracyclic triterpenes and pentacyclic triterpenes, among which tetracyclic triterpenes covered a large proportion. Some common properties were observed in the pharmacophore and binding modes. The pharmacophore map (Fig. 6a-1 and a-2) showed the 3-hydroxyl was well fitted by the hydrogen bond donor pharmacophore, meanwhile the tetracyclic triterpenes with 2-, 3-, 4- hydroxyl could have good fit with pharmacophore. The hexatomic ring consisting of atoms 8, 9, 11, 12, 13, 14 were all mapped with the hydrophobics pharmacophore. The carbonyl and carboxyl on the 22–27 positions were beneficial for hydrogen bond acceptor pharmacophore. The binding mode showed the backbone of tetracyclic triterpenes preferred to bind into the cleft region, while it appeared to interact with the strong hydrophobic interactions with surrounding residues. The side chain often substituted with carbonyl, hydroxyl and carboxyl were located in the back of the cavity, providing the possibility to be involved in the water mediated hydrogen bond bound.

Whether these saponins might inhibit NMMHC IIA ATPase activity as blebbistatin does need to be investigated in future studies.

Overall, our present work facilitates understanding of the interaction mechanism of blebbistatin with NMMHC IIA and presents an opportunity for further research on more potential inhibitors.

References

1. Song JX, Kou JP, Yu BY (2009) Recent advances of NMHCIIA in physiological and pathological functions. Prog Mod Biomed 9:3964–3979. doi:cnki:sun:swcx.0.2009-20-050
2. Clark K, Middelbeek J, Dorovkov MV, Figdor CG, Ryazanov AG, Lasonder E, van Leeuwen FN (2008) The alpha-kinases TRPM6 and TRPM7, but not eEF-2 kinase, phosphorylate the assembly domain of myosinIIA, IIB and IIC. FEBS Lett 582:2993–2997. doi:10.1016/j.febslet.2008.07.043
3. Manzanares MV, Ma XF, Adelstein RS, Horwitz AR (2009) Non-muscle myosin II takes centre stage in cell adhesion and migration. Nat Rev Mol Cell Biol 10:778–790. doi:10.1038/nrm2786
4. Conti MA, Even-Ram S, Liu C, Yamada KM, Adelstein RS (2004) Defects in cell adhesion and the visceral endoderm following ablation of nonmuscle myosin heavy chain II-A in mice. J Biol Chem 279:41263–41266. doi:10.1074/jbc.C400352200
5. Leon C, Eckly A, Hechler B, Aleil B, Freund M, Ravanat C, Jourdain M, Nonne C, Weber J, Tiedt R, Gratacap MP, Severin S, Cazenave JP, Lanza F, Skoda R, Gachet C (2007) Megakaryocyte-restricted MYH9 inactivation dramatically affects hemostasis while preserving platelet aggregation and secretion. Blood 110:3183–3191. doi:10.1182/blood-2007-03-080184
6. Arii J, Goto H, Suenaga T, Oyama M, Kozuka-Hata H, Imai T, Minowa A, Akashi H, Arase H, Kawaoka Y, Kawaguchi Y (2010) Non-muscle myosin IIA is a functional entry receptor for herpes simplex virus-1. Nature 467:859–864. doi:10.1038/nature09420
7. Liang SL, He LJ, Zhao XD, Miao Y, Gu Y, Guo CC, Xue ZF, Dou WJ, Hu FR, Wu KC, Nie YZ, Fan DM (2011) MicroRNA let-7f inhibits tumor invasion and metastasis by targeting MYH9 in human gastric cancer. PLoS One 6:e18409. doi:10.1371/journal.pone.0018409
8. Wrighton KH (2011) Autophagy: myosin II moves in on autophagosomes. Nat Rev Mol Cell Biol 12:77. doi:10.1038/nrm3053
9. Yu BY, Kou JP, Huang YL, Jiang WW, Liu JH, A target of control inflammation associated with cardiac and cerebral vascular diseases and its inhibitor drug target. China patent authorization ZL 200710024810
10. Duxbury MS, Ashley SW, Whang EE (2004) Inhibition of pancreatic adenocarcinoma cellular invasiveness by blebbistatin: a novel

myosin II inhibitor. Biochem Biophys Res Commun 313:992–997. doi:10.1016/j.bbrc.2003.12.031

11. Kovacs M, Toth J, Hetenyi C, Malnasi-Csizmadia A, Sellers JR (2004) Mechanism of blebbistatin inhibition of myosin II. J Biol Chem 279:35557–35563. doi:10.1074/jbc.M405319200

12. Gu BJ, Rathsam C, Stokes L, McGeachie AB, Wiley JS (2009) Extracellular ATP dissociates nonmuscle myosin from $P2X_7$ complex: this dissociation regulates $P2X_7$ pore formation. Am J Physiol Cell Physiol 297:430–439. doi:10.1152/ajpcell.00079.2009

13. Gu BJ, Saunders BM, Jursik C, Wiley JS (2010) The $P2X_7$-nonmuscle myosin membrane complex regulates phagocytosis of non-opsonized particles and bacteria by a pathway attenuated by extracellular ATP. Blood 115:1621–1631. doi:10.1182/blood-2009-11-251744

14. Jacobelli J, Chmura SA, Buxton DB, Davis MM, Krummel MF (2004) A single class II myosin modulates T cell motility and stopping, but not synapse formation. Nat Immunol 5:531–538. doi:10.1038/ni1065

15. Jacobelli J, Bennett FC, Pandurangi P, Tooley AJ, Krummel MF (2009) Myosin-IIA and ICAM-1 regulate the interchange between two distinct modes of T cell migration. J Immunol 182:2041–2050. doi:10.4049/jimmunol.0803267

16. Dou Y, Arlock P, Arner A (2007) Blebbistatin specifically inhibits actin-myosin interaction in mouse cardiac muscle. Am J Physiol Cell Physiol 293:1148–1153. doi:10.1152/ajpcell.00551.2006

17. Allingham JS, Smith R, Rayment I (2005) The structural basis of blebbistatin inhibition and specificity for myosin II. Nat Struct Mol Biol 12:378–379. doi:10.1038/nsmb908

18. Nicola G, Smith CA, Lucumi E, Kuo MR, Karagyozov L, Fidock DA, Sacchettini JC, Abagyan R (2007) Discovery of novel inhibitors targeting enoyl-acyl carrier protein reductase in plasmodium falciparum by structure based virtual screening. Biochem Biophys Res Commun 358:686–691. doi:10.1016/j.bbrc.2007.04.113

19. Koppole S, Smith JC, Fischer S (2006) Simulations of the myosin II motor reveal a nucleotide-state sensing element that controls the recovery stroke. J Mol Biol 361:604–616. doi:10.1016/j.jmb.2006.06.022

20. Woo HJ (2007) Exploration of the conformational space of myosin recovery stroke via molecular dynamics. Biophys Chem 125:127–137. doi:10.1016/j.bpc.2006.07.001

21. Yamanaka K, Okimoto N, Neya S, Hata M, Hoshino T (2006) Behavior of water molecules in ATPase pocket of myosin. J Mol Struct THEOCHEM 758:97–105. doi:10.1016/j.theochem.2005.10.019

22. Kawakubo T, Okada O, Minami T (2005) Molecular dynamics simulations of evolved collective motions of atoms in the myosin motor domain upon perturbation of the ATPase pocket. Biophys Chem 115:77–85. doi:10.1016/j.bpc.2004.12.049

23. Alamo L, Wriggers W, Pinto A, Bartoli F, Salazar L, Zhao FQ, Craig R, Padron R (2008) Three-dimensional reconstruction of tarantula myosin filaments suggests how phosphorylation may regulate myosin activity. J Mol Biol 384:780–797. doi:10.1016/j.jmb.2008.10.013

24. Zoghbi ME, Woodhead JL, Moss RL, Craig R (2008) Three-dimensional structure of vertebrate cardiac muscle myosin filaments. PNAS 105:2386–2390

25. Onishi H, Ohki N, Morales MF (2004) On the myosin catalysis of ATP hydrolysis. Biochemistry 43:3757–3763. doi:10.1006/jsbi.1999.4207

26. Smith CA, Rayment I (1996) X-ray structure of the magnesium (II)·ADP·Vanadate complex of the Dictyostelium discoideum myosin motor domain to 1.9 Å resolution. Biochemistry 35:5404–5417. doi:10.1021/bi00028a005

27. Tang S, Liao JC, Dunn AR, Altman RB, Spudich JA, Schmidt JP (2007) Predicting allosteric communication in myosin via a pathway of conserved residues. J Mol Biol 373:1361–1373. doi:10.1016/j.jmb.2007.08.059

28. Kawakubo T, Okada O, Minami T (2009) Dynamic conformational changes due to the ATP hydrolysis in the motor domain of myosin:10-ns molecular dynamics simulations. Biophys Chem 141:75–86. doi:10.1016/j.bpc.2008.12.014